Chemisorption of Organics on Platinum. 1. The Interstitial Electron Model

Jeremy Kua and William A. Goddard III*

Materials and Process Simulation Center, Beckman Institute (139-74), Division of Chemistry and Chemical Engineering, California Institute of Technology, Pasadena, California 91125

Received: June 8, 1998; In Final Form: August 18, 1998

Using first principles quantum mechanics (nonlocal density functional theory), we studied the bonding and electronic states for clusters of Pt atoms. These calculations suggest the interstitial electron model (IEM) in which (i) the 6s valence orbitals from the four atoms of a tetrahedron combine to form an interstitial bonding orbital at the center of the tetrahedron that is occupied by two electrons to form the interstitial electron bond (IEB), (ii) the 5d valence orbitals from each atom form a band of bonding and antibonding states sufficiently dense that the optimum occupation is high spin (Hund's rule) or nearly so, and (iii) bonds of organics to the Pt surface lead to covalent σ bonds to d orbitals localized on individual Pt atoms. This simple model explains the bonding and lowest electronic state of essentially all clusters studied. The IEM suggests that the bonding in three-dimensional face-centered cubic (fcc) systems has two electrons from each atom in the IEB, leaving the remaining eight valence electrons in d-like orbitals. For bulk Pt, this leads to a $6s^25d^8$ effective electronic configuration. The IEM suggests that the (111) surface of Pt would have a $6s^15d^9$ effective electronic configuration. This suggests that to model the chemistry of the Pt(111) surface we should use clusters leading to the $(6s)^1(5d)^9$ configuration. This suggests the interstitial electron surface model (IESM) in which a simple planar cluster with eight atoms serves to model the chemistry of the Pt(111) surface. This is used in the accompanying paper (part 2) to examine CH_x and C_2H_x species chemisorbed on Pt(111).

1. Introduction

In recent decades, there has been enormous progress toward a fundamental understanding of the nature of reactivity in organic reactions (e.g., the Woodward−Hoffmann rules) and in organometallic systems where the nature of the atomic and molecular orbitals can be used directly in explaining the reactivity. There has also been enormous progress in the characterization of chemisorption and reactions on metal surfaces (mostly based on surface science experiments). However, there has been little advance in how the orbitals of the surface control the reactions on metal surfaces. Instead, most discussions treat the metal atoms as round balls with little regard for the character of the orbitals. Such a view may be rationalized in terms of the delocalization of the molecular orbitals into bands of states where the atomic character may not be obvious. However, we believe the evidence is that chemical reactions involve localized sets of orbitals, even on metal surfaces.

To lay the foundation for developing an orbital view useful for chemical reasoning about reactions on metal surfaces, we initiated a research program examining the properties of small metal clusters and the bonding of organics to these clusters. Previous calculations on metal clusters have focused on equilibrium structures and adsorption of small molecules. Feng and Lin chose planar clusters containing from 7 to 12 Pt atoms of appropriate symmetry to bind CH_x fragments using DV-Aα methods.[1] Fahmi and van Santen used local density functional theory (DFT) to study the interaction of water and ammonia with Pt_4 and Pt_6 clusters.[2] Higher levels of theory have been applied to similar problems over the past two years. The chemisorption of CO to Pt(111) has been the subject of much theoretical investigation. Illas and co-workers[3] used complete active space self-consistent field (CASSCF) methods to study CO adsorption on the Pt_4 tetrahedron. Dumesic and co-workers[4] have used the B3LYP flavor of DFT to study single and multiple CO adsorption to a Pt_{10} tetrahedron, with application to Pt clusters supported in L-zeolite. Adsorption of atomic oxygen to similar Pt_{10} and Rh_{10} tetrahedral clusters has been studied using nonlocal DFT.[5] A theoretical study of CH_4 photodissociation has also been carried out using a Pt_n ($n = 1, 4, 6, 7, 10$) cluster model both by DFT and state-averaged CASSCF.[6] It has been suggested by theoretical studies on Pt_n clusters that when the number of Pt in the cluster reaches seven atoms, the electronic structure of the cluster becomes more metallic.[7] Smaller clusters ($n < 7$) on the other hand show vastly different electronic properties from bulk metallic platinum.

The concept of interstitial bonds in metallic bonding was suggested by McAdon and Goddard[8] based on generalized valence bond (GVB) calculations of M_n (M = Li, Na, Cu, Ag, Au). They found that, for one-dimensional systems, singly occupied orbitals are localized at each bond midpoint to form one-electron bonds. Two-dimensional systems have orbitals localized at the centers of equilateral triangles in the interior and at bond midpoints at the edge regions. They suggest that infinite systems have interstitial electrons at the center of the tetrahedra.

Our focus in studying metal clusters is to extract an orbital view of the electronic states. This led to the interstitial electron model (IEM) for the states of the metal clusters. On the basis of the IEM from metal clusters, we deduced the orbital nature expected for the infinite crystal and reasoned about the nature of the atoms on the surface of the bulk metal. This led to the idea that the surface atoms for bulk Pt prefer to have a $6s^15d^9$ electron configuration. This suggested a strategy by which small clusters could be constructed whose surface chemistry would mimic the properties of the bulk surface. We then used this

10.1021/jp9825260 CCC: $15.00
Published on Web 11/03/1998

TABLE 1: Calculated Energetics of Geometry-Optimized Platinum Clusters with NLDA-GGAII

no. Pt	geometry (symmetry)	absolute ground-state energy (hartrees)	spin	excited-state energy (kcal/mol)	total binding energy (kcal/mol)	binding energy (kcal/mol)	IBO
2	linear ($D_{\infty h}$)	−238.360 32	0	21.38	83.62	83.62	1
			1	0			
3	triangle (D_{3h})	−357.604 74	0	3.27	165.76	82.88	1
			1	0			
4	tetrahedron (T_d)	−476.843 39	3	22.12	244.27	81.42	1
			0	9.32			
			2	4.21	235		
			1	0			
4	rhombus (D_{2h})	−476.830 92	1	7.59	236.45	78.82	2
			0	3.77			
			2	0	233		
4	square (D_{4h})	−476.828 43	2	18.35	234.77	78.26	1
			0	1.45			
			1	0	233		
5	face-shared tetrahedron (D_{3h})	−596.100 39	0	11.65	334.31	83.55	2
			1	7.05			
			2	0			
5	square pyramid (C_{4v})	−596.087 37	4	18.42	328.24	82.06	3
			0	8.93			
			2	3.96			
			1	2.75			
			3	0			
6	edge-shared tetrahedra (D_{2h})	−715.346 44	0	15.42	417.47	83.50	2
			3	5.81			
			1	2.33			
			2	0			
6	triangle (D_{3h})	−715.339 36	4	46.97	413.02	82.60	3
			0	29.11			
			1	11.86			
			2	10.62			
			3	0			
6	octahedron (O_h)	−715.339 70	1	3.68	413.24	82.34	1
			0	3.10			
			2	2.88			
			4	0.09			
			3	0			
7	hexagon (D_{6h})	−834.565 54	1	24.60	483.91	80.65	3
			0	3.78			
			3	2.66			
			2	0			
9	bilayer (6.3) (C_{3v})	−1073.157 79	4	13.30	712.88	89.11	4
			3	0			
10	trilayer (6.3.1) (T_d)	−1192.429 02	5	22.54	811.81	90.20	4
			2	12.46			
			4	0.85			
			3	0			

interstitial electron surface model (IESM) to study the chemisorption and reactions on bulk Pt systems. We conclude that the reaction energetics are similar to that of bulk Pt. We find that essentially all stable strongly chemisorbed organic intermediates can be described accurately in terms of localized C−Pt σ bonds involving a tetrahedrally hybridized C orbital overlapping a localized d-like orbital on the metal.

We have more recently extended these studies to other metals including Os, Ir, Ru, Rh, and Pd and found that the same concepts apply to these systems. In this paper, we focus on Pt. Subsequent papers will examine the trends in various parts of the periodic table.

2. Platinum Clusters

We optimized the structures for clusters with up to 10 Pt atoms and carried out single-point calculations for those and additional 9−10 atom clusters. In each case, we determined the optimum spin. The energetic results are given in Table 1, and the optimum structures are shown in Figure 1. We see that the average bond distance increases gradually from 2.36 Å with Pt_2 to 2.774 Å for the central part of Pt_{10}. This compares with the experimental bond distance of 2.775 Å for bulk Pt, suggesting that the central atoms of these small clusters already have character similar to the bulk system.

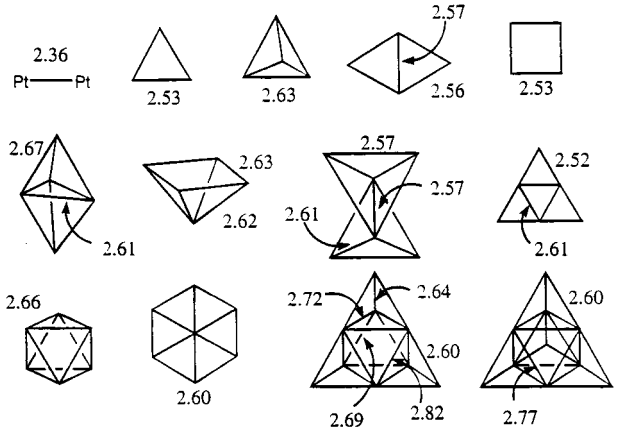

Figure 1. Optimized ground-state structures of platinum clusters, with distances in angstroms.

A remarkable result here is that the net cohesive energy of the Pt_N cluster is

$$E_{coh} \approx (N - 1)85 \text{ kcal/mol}$$

where N is the number of atoms. This suggests that each additional atom (after the first) adds the same amount to the cohesion of the system. The calculated bond energy of 83.6 kcal/mol for Pt_2 is in the range of experimental results, 65−86 kcal/mol.[9] The experimental cohesive energy for bulk Pt is 134.9 kcal/mol.[10]

For Pt_4, we find (DFT/NLDA-GGAII) the ground state to be the tetrahedron, with the rhombus being 7.8 kcal/mol higher and the square 9.5 kcal/mol higher. There is no experimental data to compare with. Using the CASSCF method, Dai[11] reports the rhombus to be more stable than the tetrahedron by 1.1 kcal/mol. With DFT in the local density approximation (LDA), Yang[12] reports the rhombus to be more stable than the tetrahedron by 1.1 kcal/mol. Using the DV-Xα methods, Ellis[13] found the square to be most stable (by 10 kcal/mol over the rhombus). On the basis of extended Hückel calculations, Bigot[14] reported the tetrahedron to be most stable (10.4 kcal/mol below rhombus). Of these previous calculations, only Dai and Ellis seem to have optimized the spin. Of these methods, we expect B3LYP/DFT to be most accurate.

For Pt_6, we find that the edge-shared tetrahedron is lowest (4.45 kcal/mol better than the planar structure and 4.23 kcal/mol better than the octahedron). No previous predictions seem to have considered this structure. For Pt_{10} we find a three-layer structure (6 + 3 + 1 atoms per layer), which leads to a super tetrahedron with six closest packed atoms on each face.

2.1. Interstitial Electron Model. For linear Pt_2, the gound state has two electrons in a symmetric (bonding) combination of 6s orbitals and 20 − 2 = 18 electrons distributed among the two 5d-like orbitals, leading to a spin $S = 1$ (triplet) state. The antibonding combination of the 6s orbital is much higher, as are various combinations of 6p orbitals. This is shown in Figure 2a.

Similarly, for triangular Pt_3, the ground state has two electrons in a symmetric (bonding) combination of three 6s orbitals and 30 − 2 = 28 electrons distributed among the 15 5d-like orbitals, leading to a spin $S = 1$ (triplet) state. The two antibonding combinations of the 6s orbitals are much higher, as are various combinations of 6p orbitals. This is shown in Figure 2b.

Similarly, for tetrahedral Pt_4, the ground state has two electrons in a symmetric (bonding) combination of four 6s orbitals and 40 − 2 = 38 electrons distributed among the 20 5d-like orbitals, leading to a spin $S = 1$ (triplet) state. The three antibonding combinations of the 6s orbitals are much higher as are various combinations of 6p orbitals. This is shown in Figure 2c.

These results are summarized in Figure 3. It is because 6s orbitals on adjacent Pt atoms have much higher overlap than do 5d orbitals that the antibonding combinations of 6s orbitals are so much higher than the antibonding 5d orbitals. Because these clusters are being used to model the extended Pt(111) surface, we calculated the energies of different spin states of these clusters at the bulk platinum distances (Pt−Pt = 2.775 Å) using the B3LYP level of DFT (see Table 2). For comparison, the NLDA-GGAII energies are tabulated in Table 3. Differences between the levels of theory and between single-point and geometry-optimized clusters are discussed in Appendix C.

For the larger clusters, Pt_N, we find similar interstitial bond orbitals (IBO) formed from symmetric combinations of 6s orbitals of tetrahedra or triangles to dominate the bonding, leaving the remaining ($10N$ − 2 × IBO) electrons to be sprinkled over the $5N$ d orbitals. The maximum number of unpaired spins for such a system is 2 × IBO, leading to a net spin of S = IBO. Usually we find this maximum spin case to be the ground state (Hund's rule). Figure 4 shows the IBO calculated for the various clusters. Here, we see that the IBO tend not to occupy adjacent triangles or tetrahedra. This is because the Pauli principle, requiring that the orbitals be orthogonal, would force the IBO to incorporate 5d or 6p character.

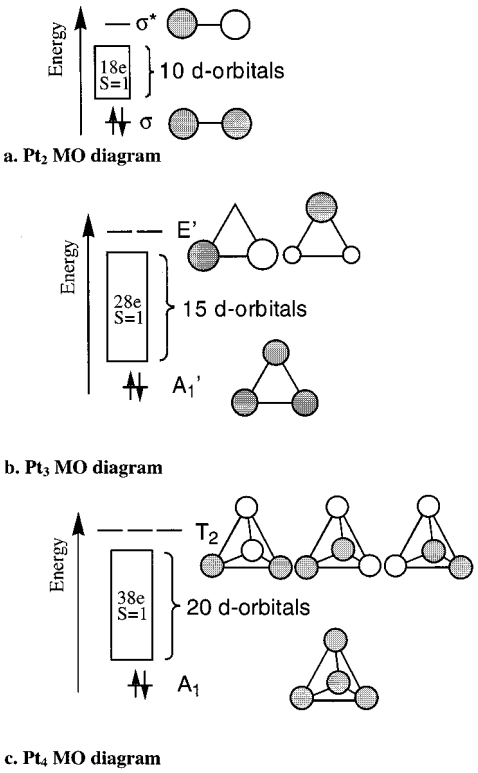

Figure 2. Examples of the application of the IEM to predict the spin in Pt clusters.

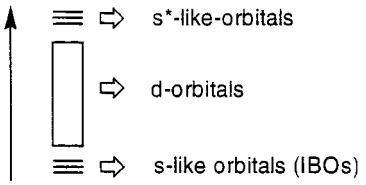

Figure 3. Schematic energy diagram for platinum clusters.

These results suggest a simple procedure for predicting the ground-state spin of a cluster.

1. Determine the number of IBO in the cluster.
2. Occupy each IBO with two electrons.
3. Since the antibonding combination of s orbitals is left unoccupied, the remaining electrons are filled into d orbitals.
4. Using the simple assumption that the d orbitals are close in energy, we can apply Hund's rule to determine the predicted ground spin state.

A brief discussion of the number and location of IBO is in order, since this determines the ground spin state of the cluster. Figure 4 shows the number and location of IBO in each of these clusters.

The Pt_4 rhombus has two equivalent triangles each containing an IBO; this leads to $S = 2$. The Pt_4 square has one IBO in its center, which leads to $S = 1$.

TABLE 2: Single-Point Energy Calculations of Pt_N Clusters at Bulk Distances with B3LYP

N	geometry (symmetry)	ground-state energy (hartrees)	spin	excited-state energy (kcal/mol)	IBO
2	linear ($D_{\infty h}$)	−238.221 01	0	20.41	1
			1	0	
3	triangle (D_{3h})	−357.405 22	0	2.05	1
			1	0	
4	tetrahedron (T_d)	−476.591 98	0	14.55	
			2	7.63	
			1	0	
4	rhombus (D_{2h})	−476.554 84	0	2.40	2
			1	0.54	
			2	0	
4	square (D_{4h})	−476.548 21	2	12.18	1
			1	2.92	
			0	0	
5	face-shared tetrahedron (D_{3h})	−595.770 21	0	16.99	2
			3	13.02	
			1	5.56	
			2	0	
5	square pyramid (C_{4v})	−595.768 39	4	27.65	3
			2	3.51	
			3	0	
6	edge-shared tetrahedron (D_{2h})	−714.936 13	0	17.64	2
			1	5.34	
			3	4.17	
			2	0	
6	triangle (D_{3h})	−714.912 09	4	34.02	3
			2	10.41	
			3	0	
6	octahedron (O_h)	−714.932 19	5	40.41	4
			2	7.46	
			3	4.79	
			4	0	
7	hexagon (D_{6h})	−834.089 03	1	28.32	3
			4	25.11	
			2	21.68	
			3	0	
9	bilayer (6.3) (C_{3v})	−1072.507 63	5	30.97	4
			2	11.58	
			3	0.40	
			4	0	
9	bilayer (5.4) (C_{4v})	−1072.477 19	3	7.12	2
			1	4.40	
			2	0	
10	bilayer (7.3) (C_{3v})	−1191.675 06	5	13.81	
			2	12.95	4
			3	4.68	
			4	0	
10	trilayer (6.3.1) (T_d)	−1191.697 44	5	24.92	4
			3	16.67	
			4	0	
10	trilayer (5.4.1) (C_{4v})	−1191.669 92	5	11.61	4
			3	10.09	
			4	0	

For Pt_5 with face-shared tetrahedra, there is an IBO in each of the two equivalent tetrahedra, leading to $S = 2$. The Pt_5 square pyramid has three IBO, one located on the square face and two located in the two alternate triangular faces.

In the Pt_6 triangle, we find one IBO in each of the edge triangles, leading to $S = 3$. The central triangle does not have an IBO. This cluster illustrates the feature of alternation of IBO that we will find in the larger clusters. The edge-shared tetrahedra Pt_6 cluster has two equivalent tetrahedra, and consequently there are two IBO ($S = 2$). The octahedron has four IBO in alternate triangular faces, leading to $S = 4$.

The Pt_7 hexagon also shows alternation. It has three IBO in alternate triangles, leading to $S = 3$. An equivalent structure has the three IBO in the *other* three triangles (see discussion).

The Pt_9 (6.3 bilayer) has an $S = 4$ ground state. IBO are located in three of the tetrahedra. The fourth IBO is associated with the face of the octahedron, satisfying the alternating pattern (on the three-atom face).

The Pt_{10} tetrahedron has four IBO located in the four tetrahedra that are arranged at the alternate faces of the central octahedron, and $S = 4$ as expected.

On the whole, the *S* values calculated for these clusters from quantum mechanics match remarkably well with the *S* values predicted from the IEM.

The only case that does not is the Pt_4 square. Here, the IEM suggests $S = 1$, whereas the value calculated using B3LYP is $S = 0$ (with $S = 1$ higher by 2.9 kcal/mol). [The NLDA-GGAII flavor of DFT gives a ground state with $S = 1$ as expected from IEM.] However, we find that the orbitals for $S = 0$ and $S = 1$ are essentially the same (with one IBO), indicating that the $S = 0$ arises from spin pairing of the d electrons in the two highest d-like orbitals of the $S = 1$ state (Hund's rule is not

TABLE 3: Single-Point Energy Calculations of Pt_N Clusters at Bulk Distances with NLDA-GGAII

N	geometry (symmetry)	ground-state energy (hartrees)	spin	excited-state energy (kcal/mol)	IBO
2	linear ($D_{\infty h}$)	−238.328 92	0	20.69	1
			1	0	
3	triangle (D_{3h})	−357.573 61	0	4.79	1
			1	0	
4	tetrahedron (T_d)	−476.825 86	0	10.06	1
			2	7.31	
			2	0	
4	rhombus (D_{2h})	−476.796 16	1	7.49	2
			0	4.15	
			2	0	
4	square (D_{4h})	−476.779 74	0	6.40	1
			2	1.47	
			1	0	
5	face-shared tetrahedron (D_{3h})	−596.084 82	3	17.90	2
			0	14.70	
			1	5.97	
5	square pyramid (C_{4v})	−596.071 40	4	18.49	3
			2	2.59	
			3	0	
6	edge-shared tetrahedra (D_{2h})	−715.321 32	0	12.68	2
			3	4.66	
			1	2.14	
			2	0	
6	triangle (D_{3h})	−715.302 76	4	37.86	3
			2	12.53	
			3	0	
6	octahedraon (O_h)	−715.320 98	5	40.92	4
			2	1.26	
			4	0.46	
			3	0	
7	hexagon (D_{6h})	−834.525 55	1	15.14	3
			4	11.38	
			2	8.82	
			3	0	
9	bilayer (6.3) (C_{3v})	−1073.122 61	5	25.07	4
			2	9.88	
			3	0.01	
			4	0	
9	bilayer (5.4) (C_{4v})	−1073.092 44	3	10.68	2
			1	6.49	
			2	0	
10	bilayer (7.3) (C_{3v})	−1192.347 80	5	15.39	4
			4	2.66	
			3	0.90	
			2	0	
10	trilayer (6.3.1) (T_d)	−1192.399 52	5	27.49	4
			3	10.01	
			4	0	
10	trilayer (5.4.1) (C_{4v})	−1192.346 46	5	11.35	4
			3	3.51	
			4	0	

quite satisfied). We expect this effect to be more apparent at shorter distances where it becomes more favorable to spin-pair electrons in the high-lying d orbitals. Such violations of Hund's rule are expected to occur more in larger clusters. A general schematic of this is shown in Figure 5. A comparison of different levels of theory is made in Appendix B, and a comparison of energetics for optimized versus single-point cluster calculations is discussed in Appendix C.

2.2. Implications of the IEM for Bulk Pt. We wish to extrapolate the results from the cluster calculations to predict the bonding in bulk and surface platinum. A platinum crystal has a closed cubic-packed (ccp) structure with a face-centered cubic (fcc) unit cell. Each cubic unit cell consists of four platinum atoms, eight tetrahedra, and four octahedra. Figure 6 shows the fcc unit cell and a view of the central octahedron (white spheres), which has each of its eight triangular faces capped (with black spheres) to form the eight tetrahedra. The remaining space of the cube is taken up by three octahedra formed by half octahedra on each of the six faces of the cube.

Since the crystal is made up of edge-sharing tetrahedra but also contains octahedra sharing faces with tetrahedra, an IBO has four possible locations: (a) in the center of a formal Pt−Pt bond, (b) in the center of a triangular face, (c) in the center of a tetrahedron, or (d) in the center of an octahedron. Our calculations suggest that for bulk Pt there would be doubly occupied IBO *located in half the tetrahedra.*[15] The Pt_6 triangle and octahedron and the Pt_7 hexagon show alternation of the IBO. The Pt_9 and Pt_{10} clusters (along with Pt_4 tetrahedron) suggest that the IBO are located in tetrahedra rather than octahedra. To confirm the validity of our suggestion, we did single-point energy calculations to determine the ground spin states for three larger clusters (see Figure 7) at the Pt bulk distances (Pt−Pt = 2.775 Å). The ordering of spin states is shown in Table 1c.

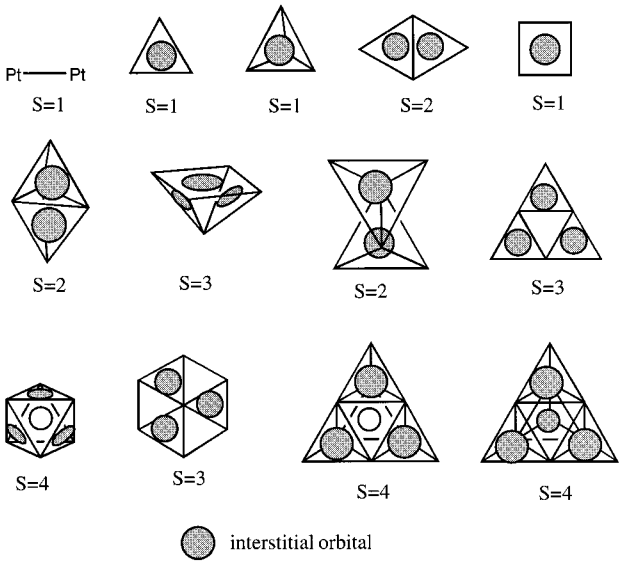

Figure 4. IBO and *S* values predicted by IEM for platinum clusters.

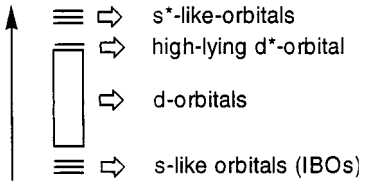

Figure 5. Schematic energy diagram showing pairing of electrons to leave high-lying d* orbitals unoccupied.

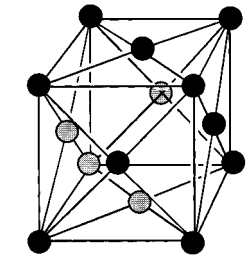

a. fcc unit cell

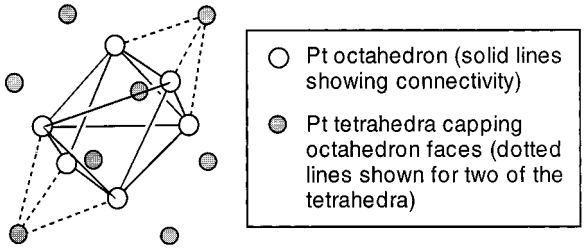

b. Location of octahedra and tetrahedra

Figure 6. Unit cell of platinum (fcc) showing face-shared octahedra and tetrahedra.

The first of these is a Pt_9 (5.4) bilayer cluster that is half of the fcc unit cell. The five-atom face forms the top layer and the second layer has four atoms. Geometrically, this structure is a half octahedron with four tetahedra capping the four adjacent triangular faces. The calculated ground state of this cluster is $S = 2$; i.e., two IBO are present and located in two of the four tetrahedra. The second cluster is a Pt_{10} (5.4.1) trilayer, which differs from the first cluster by having an additional atom in the third layer to complete the octahedron. From our small cluster calculations, we predicted that this adds two IBO on two of the triangular faces of the bottom half of the octahedron. Indeed, calculations give us $S = 4$ as the ground state, indicating that this cluster has four IBO. The third cluster, the Pt_{10} (7.3) bilayer, has a hexagonal layer of seven atoms with three additional atoms in the second layer to form one inner tetrahedra, three outer tetrahedra, and three half octahedra. If the IBO are located in the tetrahedra, we expect to find an IBO in each of the three outer tetrahedra plus one in the central tetrahedra. If instead they are in the half octahedra, we would expect to find six IBO (two for each of the half octahedra). Our cluster calculation gives $S = 4$; i.e., three IBO are located in the outer tetrahedra and one in the inner tetrahedra. Thus, the IBO prefer tetrahedra.

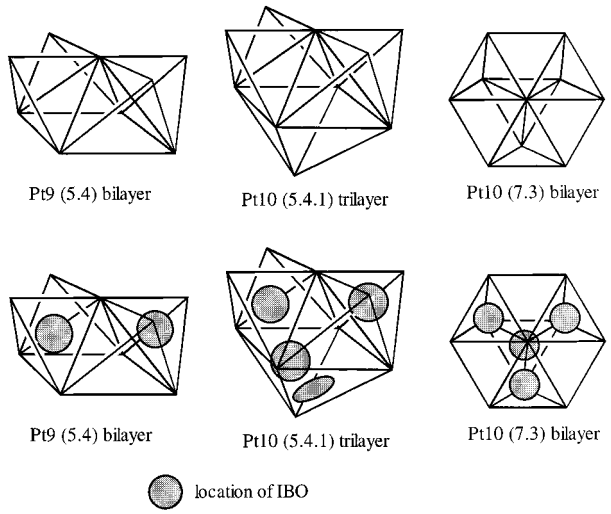

Figure 7. Geometries of three larger Pt_9 and Pt_{10} clusters.

We now return to the unit cell of platinum. Each unit cell has four platinum atoms and eight tetrahedra. Therefore, each platinum atom is associated with two tetrahedra. Since there are IBO in half the tetrahedra, each platinum atom has one IBO associated with it. We previously showed that IBO are doubly occupied and represent the in-phase combination of s orbitals. Since platinum has 10 valence electrons, the model predicts that bulk platinum has a $6s^25d^8$ electronic configuration.

The band structure of platinum has been determined by angle-resolved ultraviolet photoemission spectroscopy (ARUPS) with general agreement with fully relativistic self-consistent calculations.[16] The lowest valence band (mostly s character) does not cross the Fermi level, suggesting an electronic configuration close to s^2d^8, in agreement with IEM predictions. However, calculations of the d occupancy vary significantly. Linear augmented Slater-type orbital methods suggest that $d^{n-1}s^2$ configurations predominate in the 5d row.[17] Platinum is calculated to have a d occupancy of 8.1−8.3. A recent Compton profile study with calculations based on the renormalized free-atom (RFA) model yielded a d occupancy of 9.2 for platinum.[18]

2.3. Implication of the IEM for the (111) Surface of Bulk Pt. We will consider the Pt(111) surface, since the most experimental data is available for this surface. To form the (111) surface for the crystal involves cleaving of one tetrahedra per surface atom (see Figure 8). [Each surface atom of the two new surfaces is shared by four tetrahedra that are cleaved, each of which is counted four times.] Since IBO are located in half the tetrahedra, then the surface atoms each must accommodate one additional electron in the d shell. This leads to the $6s^15d^9$ electronic configuration, with the s electron involved in IBO in half the tetrahedra involving the subsurface tetrahedra. This is illustrated in Figure 9. As a result, the IEM suggests that each

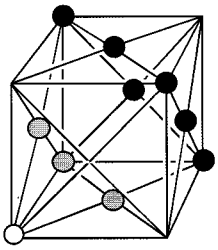

a. fcc unit cell with (111) planes shown

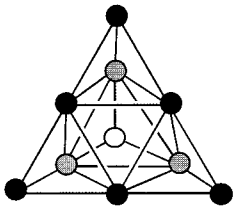

b. view along (111) axis: the Pt_{10} (6.3.1 trilayer) cluster

Figure 8. Unit cell of platinum illustrating derivation of clusters corresponding to the Pt(111) plane.

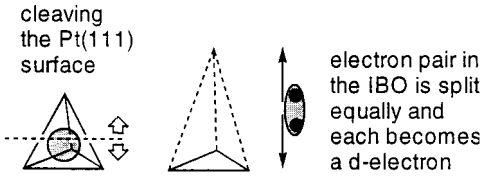

Figure 9. Illustration showing breaking of an IBO when a tetrahedron is cleaved.

platinum atom on the (111) surface has the $6s^15d^9$ configuration.

The IEM suggests an explanation for the site preference of a hydrogen atom adsorbed on Pt(111). HREELS experiments show that that H atom binds to the fcc sites of Pt(111) with a binding energy of 60 kcal/mol (at high coverage).[19] The (111) surface is composed of two different types of triangles depending on the location of the atoms in the second layer. If there is an atom directly below the triangle, this means that the triangle is a tetrahedral face and hence a hcp site. If instead there is no atom in the second layer directly below the triangle, then it is an octahedral face and hence a fcc site. This is illustrated by the Pt_9 cluster shown in Figure 10.

Consider what *previously* occupied these two sites. Before the surface at the (111) plane was cleaved, there used to be a tetrahedron sitting above an octahedral face and an octahedron sitting above a tetrahedral face (see Figure 11). Above the octahedral face (fcc site), there used to be an IBO, which has now been cleaved leaving an additional d electron available for adsorbate binding at this site. The tetrahedral face (hcp site) does not have this, since an octahedron used to be above this site. This predicts that hydrogen, with a single electron in its spherical 1s orbital, will bind preferentially at fcc sites over hcp sites.

2.4. Clusters to Model the (111) Surface. The above analysis suggests criteria for clusters to serve as good models for Pt(111). First, the clusters should have an electronic configuration close to the predicted $6s^15d^9$ electronic configuration. This criteria is met by clusters having half the number of IBO as there are atoms in the cluster. Second, the cluster should be able to model two types of triangular faces. This criteria is met by clusters having at least two inequivalent triangles on a surface (the Pt_7 hexagon has all equivalent triangles that would not work). The planar Pt_6 triangle meets these criteria but does not provide an adequate site for on-top

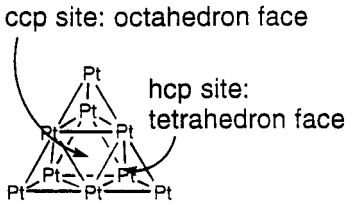

Figure 10. Pt_9 (6.3) bilayer cluster illustrating fcc and hcp sites.

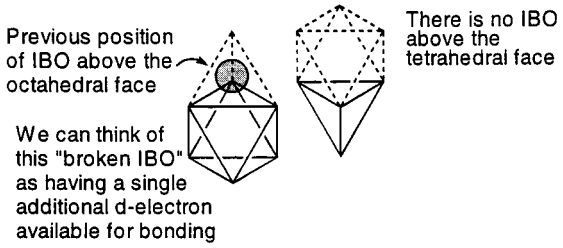

Figure 11. Illustration of *previous* location of IBO above fcc and hcp sites.

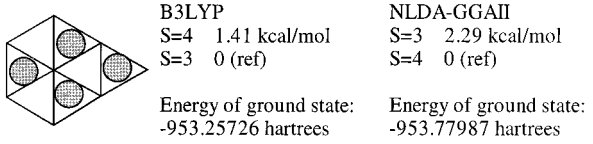

Figure 12. Pt_8 cluster proposed as a model for Pt(111).

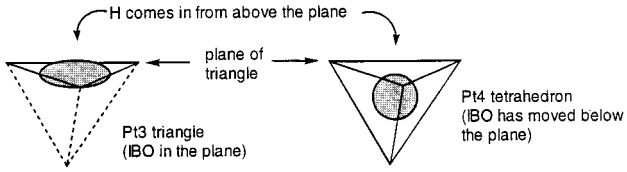

Figure 13. Position of the IBO in the Pt_3 triangle and Pt_4 tetrahedron.

binding. Thus, we consider the Pt_8 planar cluster to be the smallest cluster suitable for examining the chemistry of the fcc surfaces. This is the smallest cluster allowing all types of surface sites to be probed. Figure 12 shows this cluster and the calculated relative energies at the bulk Pt−Pt distance. The $S = 3$ state is calculated to be 1.4 kcal/mol lower in energy than the $S = 4$ state. This is due to spin pairing of d orbitals, which leaves the highest-lying d orbital unoccupied. There are still four IBO in this cluster.

2.5. Planar and Bilayer Clusters: An IEM View. In this section, we present an IEM view for understanding some biases inherent in using planar and bilayer clusters. The theory presented here uses binding of a hydrogen atom to platinum clusters as the prototype. Our calculations of H−Pt clusters support the IEM view and are presented in part 2 of this paper.

The smallest cluster having a 3-fold site is the Pt_3 triangle. We expect the H 1s orbital to overlap well with the IBO in the center of the triangle. This is the most simplified case of H binding to an "fcc-like" site (see Figure 11). The reason it is "fcc-like" is because it only approximates the fcc site, as we shall see later in the explanation. Our calculations show that H binds stably to Pt_3 at the capped (3-fold) site. However, H does not bind to the capped site of the Pt_4 tetrahedron. This is because the IBO is no longer on a triangular face but is now located in the center of the tetrahedron. Figure 13 illustrates that adding the fourth atom to the Pt_3 triangle results in the IBO "sinking" below the surface plane. There is now poor overlap between a H 1s orbital and the IBO. As we have discussed in the previous section, tetrahedral faces represent hcp sites, and so these sites are not favorable for H binding.

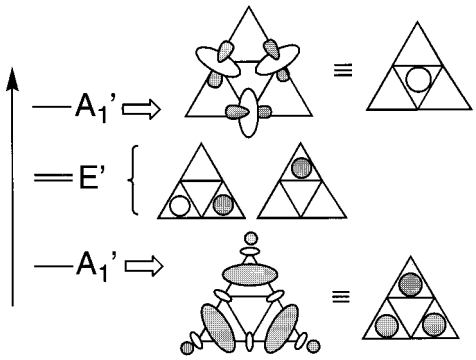

Figure 14. Lowest valence orbitals of Pt_6 planar cluster.

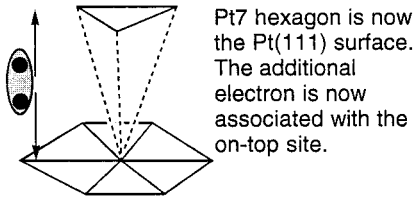

Figure 15. Cleaving of a tetrahedron favoring the on-top site.

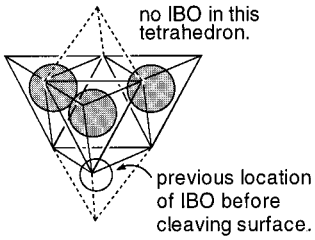

Figure 16. IBO in the Pt_9 cluster distinguishing the two fcc sites.

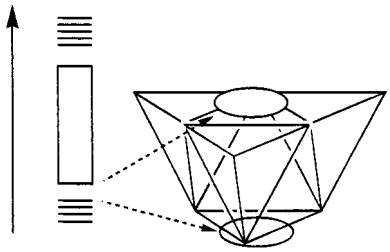

Figure 17. Schematic of valence orbitals in Pt_9 showing the different character of the orbitals at the fcc sites.

Consider now the Pt_6 planar triangle that meets the two important criteria for a cluster modeling the (111) surface (that is it has two different types of 3-fold sites and a net $6s^1 5d^9$ electronic configuration). The four lowest orbitals of this cluster are shown in Figure 14. The three lowest orbitals (A_1' and E′) have more s character, while the higher energy A_1' orbital has more d character. The three IBO are also located in the three outer triangles. Notice that the d-like A_1' orbital would also overlap with a H 1s orbital in the 3-fold site of the central triangle (and indeed we find this in our calculations).

We add three Pt atoms to form a second layer by placing them directly underneath the three outer triangles to form three tetrahedra. This leads to the Pt_9 (6.3) bilayer cluster. The three IBO in the outer triangles now "sink below the surface" in the same way that adding an additional Pt atom to the Pt_3 triangle to form a tetrahedron causes the IBO to move to the middle of the tetrahedron. Adding this second layer has no effect on the d character orbital in the central triangle (an octahedral face), which will still have good overlap with a H 1s orbital at the surface. This is why the octahedral face (fcc site) is still favorable for H binding.

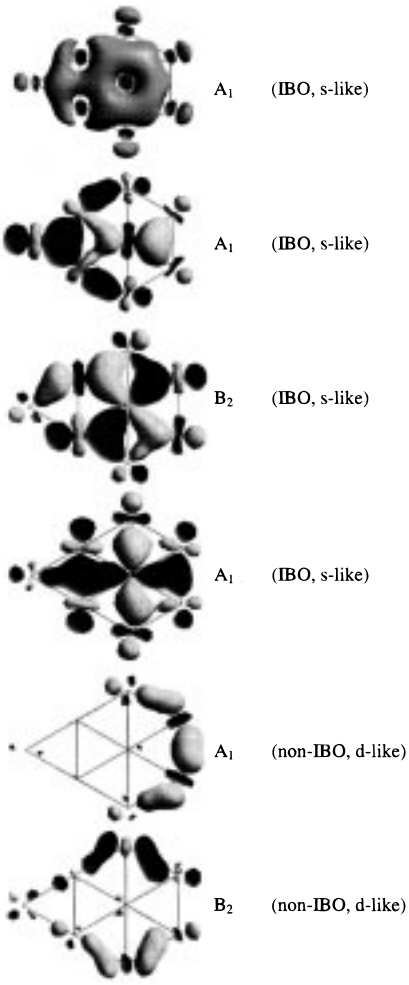

Figure 18. Six lowest valence occupied orbitals of Pt_8.

Figure 9 seems to suggest that the fcc sites are favorable for binding H because a broken IBO from a cleaved tetrahedron above this site results in an additional unpaired electron available for bonding. The same argument can be used to favor an on-top site (see Figure 15). When a tetrahedron and its corresponding IBO are cleaved, the electron pair is split homolytically between the two new "surfaces". One is associated with an on-top site, and the other is associated with a 3-fold site. This is probably not significant on the extended surface, where you end up having an average of one additional unpaired electron per surface atom. However, in a cluster, it is something that we need to be concerned about. We will now proceed to explain that the on-top site has a favorable bias in a planar cluster.

Consider now the Pt_9 (6.3) bilayer cluster (see Figure 16). The orientation of the tetrahedra containing the IBO is fixed in this cluster. The result of this is that the two opposite 3-fold faces of the central octahedron, which both model fcc sites, are not the same. If we consider two imaginary tetrahedra that would have previously occupied these two different faces, the model predicts that since half the tetrahedra are occupied by IBO there *was* an IBO in the bottom tetrahedron but not in the top one. This predicts that the fcc site formed by the three-atom surface (the bottom surface of the bilayer cluster) is favorable for H binding. The fcc site on the six-atom face is not favorable. Upon examining the orbitals, we see that both the fcc sites have potentially good overlap with the H 1s orbital. The significant difference is that overlap with the bottom face

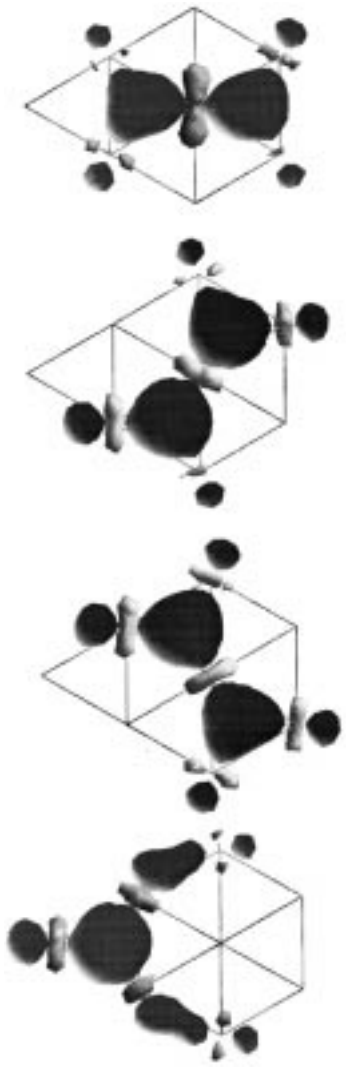

Figure 19. Pipek−Mezey localization of Pt_8 IBO.

would be with orbitals of mostly s character; overlap with the top face would be with orbitals of mostly d character (see Figure 17). Our calculations of H at these two positions (presented in part 2) are in agreement with this analysis.

Next, consider the octahedron in the center of the Pt_9 bilayer cluster. If we look down on the face of the six-atom surface, we see that the IBO are located underneath triangular faces. If instead we look up on the three-atom surface, we see that the IBO are now located underneath atom centers and not triangle centers. In a planar cluster, the IBO are located in the center of triangles. Hence, the fcc sites that do *not* have IBO are more like the fcc sites of the six-atom face of the Pt_9 cluster rather than the three-atom face. A planar cluster biases for the on-top site because, in having its IBO located in triangles, it presumes the orientation of tetrahedra containing IBO to be facing in such a way that the *points* of the tetrahedra point below the surface into the bulk. Hence, atom centers rather than 3-fold sites would have the additional associated electron from bonding after cleaving an IBO. The situation in the planar cluster therefore resembles the situation in Figure 15 rather than Figure 9, and we expect a bias in favor of the on-top site. Our calculations with H (part 2) do indeed show a small bias for the on-top site. This leads to the conclusion that the planar clusters have two different kinds of triangles that do not quite model the fcc and hcp sites, respectively. Rather they model two different kinds of fcc sites, one that allows overlap with

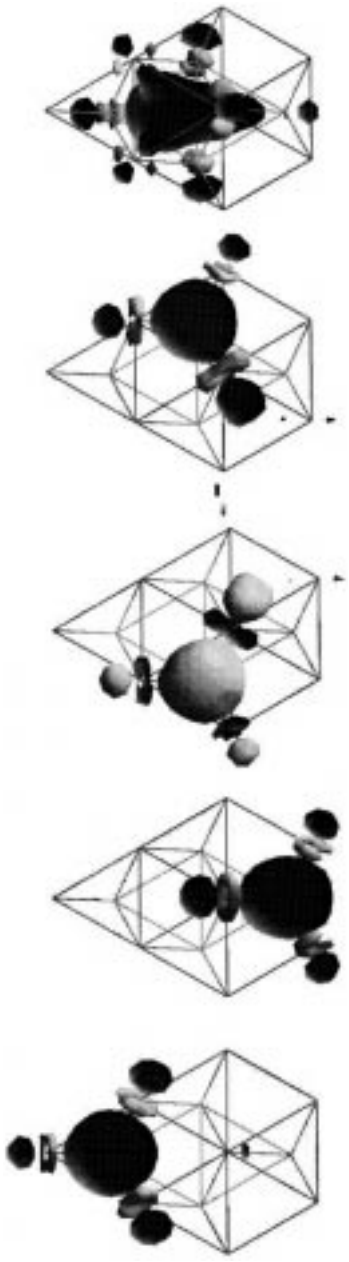

Figure 20. Pipek−Mezey localization of Pt_{12} (8.4) IBO.

the "s-like" orbitals and the other with "d-like" orbitals. The bilayer clusters are also similarly biased because of the fixed orientation of the tetrahedra inherent in such a cluster. Although we have these biases, our subsequent calculations show that the Pt_8 cluster seems quite adequate in describing the binding of hydrocarbon species to Pt(111) and the small size of the cluster is well compromised by the high level of theory used in the calculation.

In small three-dimensional clusters such as the Pt_4 tetrahedron and the Pt_6 edge-shared tetrahedra, the IBO are located in the center of tetrahedra. Each of these tetrahedral IBO is doubly occupied. If we consider the two-dimensional high-symmetry Pt_7 hexagon which has three IBO, following the same rules we would assign doubly occupied IBO to alternate triangles. However, an equivalent "resonance" structure is also present whereby the other three alternate triangles are occupied. This model would suggest six singly occupied interstitial orbitals, one in each of the triangles, echoing the model proposed by McAdon and Goddard.[8] This is equivalent to having three doubly occupied IBO in two resonant structures. The electron

TABLE 4: State Splittings (kcal/mol) for the Platinum Atom

configuration	exptl[a]	NLDA-GGAII[b]	B3-GGAII[c]	B3LYP[d]	LDA/VWN[e]	HF
s^2d^8 (^{3}F)	14.7	14.58	14.86	17.48	15.77	12.29
d^{10} (^{1}S)	11.0	12.43	12.84	12.61	9.47	26.12
s^1d^9 (^{3}D)	0	0	0	0	0	0
RMS error	0	1.28	1.54	2.27	1.32	15.31
exact exchange		none	Becke3	Becke3	none	full
exchange potential		Slater/GGA-II	Slater/Becke88	Slater/Becke88	Slater	none
local correlation		PW-91	PW-91	VWN	VWN	none
nonlocal correlation		GGA-II	GGAII	LYP	none	none

configuration remains unchanged, since the number of electrons in IBO remains the same in both pictures.

In our model Pt_8 cluster, there are four IBO formed from orbitals of predominantely s character (Figure 18). The first two d-like orbitals are also shown for comparison. The four s-like orbitals distinctly show electron density in the interstitial positions, a feature absent in the d-like orbitals. A Pipek−Mezey localization[20] of these orbitals is shown in Figure 19. The three orbitals in the hexagon part of the cluster are delocalized over two triangles each, just like the resonance structures of the Pt_7 hexagon. The fourth IBO in the outer triangle is doubly occupied. In total, there are still eight IBO electrons (s-like), giving rise to the desired s^1d^9 configuration. Figure 20 shows the five localized IBO in the Pt_{12} (8.4) bilayer cluster. Four of the doubly occupied IBO are located in the four tetrahedra of the same orientation. The last IBO is delocalized over the octahedron and the remaining tetrahedra. The electron configuration of this cluster is $s^{0.83}d^{9.17}$ since there are 10 s-like electrons in a 12-atom cluster.

3. Conclusion

We have studied the bonding in platinum clusters using nonlocal density functional methods employing a relativistic effective core potential. The ground-state spins of the clusters can be explained using the IEM. The essence of the model is the presence of low-lying IBO formed from the in-phase combination of the 6s orbitals. The corresponding out-of-phase combinations are very high in energy and left unoccupied. These two sets of orbitals sandwich a band of d orbitals. Our cluster calculations suggest that IBO are located in half the tetrahedra in platinum. Thus, the IEM predicts that bulk platinum has a $6s^25d^8$ electronic configuration and surface platinum on Pt(111) has a $6s^15d^9$ configuration. IEM also provides an explanation for the adsorption preference of H for the 3-fold fcc sites over the hcp sites. We propose the use of a Pt_8 planar cluster to model chemical reactions on Pt(111) based on its electronic configuration and ability to model the necessary sites corresponding to the (111) surface. Inherent biases in the planar and bilayer clusters are explained by the IEM. However, our computational results of chemisorption (part 2), in good agreement with experimental results, suggest that the small size of this cluster is compensated by the high level of theory used in our calculations.

Acknowledgment. The research was funded by the NSF (CHE 95-22179). The facilities of the MSC are also supported by grants from DOE-ASCI, BP Chemical, Beckman Institute, Seiko-Epson, Exxon, Owens-Corning, Asahi Chemical, Chevron Petroleum Technology Co., Chevron Chemical Co., Chevron Research and Technology Corp., and Avery-Dennison. Some calculations were carried out at the NCSA, University of Illinois.

Appendix A

Computational Methods. Calculations were carried out with nonlocal density functional theory (DFT) using the NLDA-GGAII method, which uses the Slater local exchange functional[21] and the Perdew−Wang local correlation functional with Perdew−Wang generalized gradient approximation (GGA-II) nonlocal correlation functionals.[22] The choice of this nonhybrid method was based on comparing the calculated energy splitting values of the three lowest energy states of platinum with experimental values (see Table 4). The experimental splitting energies being compared to have been averaged over spin orbitals to cancel the effects of spin−orbit coupling.[23]

All ab initio calculations were done using the PS-GVB (v2.35) and Jaguar programs.[24] The basis set used for platinum is the Hay and Wadt 18-electron relativistic effective core potential.[25] For carbon and hydrogen, the 6-31G** basis set was used.

Appendix B

Comparison of Different Methods. Tables 2 and 3 compare results from two types of DFT calculations (each including the GGA), NLDA-GGAII and B3LYP. The two methods give very similar results for the ordering of the spin states and the calculated ground state of the clusters. Generally, B3LYP gives larger energy splittings for the various states of a given cluster. Exceptions are Pt_2, Pt_3, Pt_4 rhombus, Pt_5 face-shared tetrahedron, and Pt_9 (5.4) bilayer. In these fives cases, B3LYP energetics are just slightly smaller in magnitude (2 to 3 kcal/mol) than the NLDA-GGAII numbers.

Three clusters show a difference in the ordering of the spin states. The Pt_4 square has $S = 1$ as the ground state (as predicted by IEM) using NLDA-GGAII. With B3LYP, the $S = 1$ state is 2.92 kcal/mol higher in energy than the $S = 0$ state. An examination of the orbitals shows that the $S = 0$ state leaves the highest d-like antibonding orbital (an A_{2g} state) unoccupied. The lowest bonding valence orbital is the only one with dominant s-like bonding character, with the IBO located in the center of the square.

The Pt_6 octahedron using NLDA-GGAII has $S = 4$ a mere 0.46 kcal/mol above the $S = 3$ state. Again, this is due to the pairing up of d electrons to unoccupy high-lying d orbitals.

Pt_{10} (7.3 bilayer) has $S = 2$ as the ground state using NLDA-GGAII. The $S = 3$ and $S = 4$ orbitrals are very close in energy (0.90 and 2.66 kcal/mol, respectively). Once again, the lowering of S is due to unoccupation of high-lying d-orbitals. In these latter two cases, B3LYP is in agreement with the IEM predicted value of $S = 4$ for both these clusters.

Appendix C

Effect of Structure Optimization. Tables 1 and 3 show the results of geometry-optimized clusters compared to the single-point clusters at bulk Pt distances using NLDA-GGAII; we see good agreement again between these two sets of values.

A notable exception is the Pt_7 hexagon where $S = 2$ is the calculated ground state of the optimized cluster. The shorter Pt−Pt distances in the geometry-optimized cluster make it more favorable to pair up two of the electrons occupying high-lying d orbitals.

We expect more pairing of d orbitals for larger more bulklike clusters. As fewer of the atoms are at *corners*, it becomes more favorable to pair up the spins (see Figure 5).

Similar results are obtained for the octahedral-based clusters, Pt_6 octahedron, Pt_9 (6.3) bilayer, and Pt_{10} (5.4.1) trilayer. $S = 3$ is the calculated ground state for the geometry-optimized clusters. The IEM predicts $S = 4$ to be the ground state of these clusters. In the high-symmetry Pt_6 octahedron and Pt_{10} tetrahedron, the $S = 4$ state lies less than 1 kcal/mol higher in energy.

For geometry-optimized Pt_9 (6.3 bilayer), the $S = 4$ state is 13.30 kcal/mol higher in energy than the $S = 3$ state. However, the octahedron is distorted in this cluster because of the lowered symmetry. From single-point calculations for this cluster (both methods), we find that the gap between the $S = 3$ and $S = 4$ states is less than 1 kcal/mol. The very small gap (less than 1 kcal/mol) indicates the metallic character of the cluster, a phenomena that is expected as we go to larger clusters.[7]

References and Notes

(1) Feng, K. A.; Lin, Z. D. *Appl. Surf. Sci.* **1993**, *72*, 139.
(2) Fahmi, A.; van Santen, R. A. *Z. Phys. Chem.* **1996**, *197*, 203.
(3) Illas, F.; Zurita, S.; Marquez, A. M.; Rubio, J. *Surf. Sci.* **1997**, *376*, 279.
(4) Watwe, R. M.; Spiewak, B. E.; Cortright, R. D.; Dumesic, J. A. *Catal. Lett.* **1998**, *51*, 139.
(5) Chen, M.; Bates, S. P.; van Santen, R. A.; Friend, C. M. *J. Phys. Chem. B* **1997**, *101*, 10051.
(6) Akinaga, Y.; Taketsugu, T.; Hirao, K. *J. Chem. Phys.* **1997**, *107*, 415.
(7) Xu, W.; Schierbaum, K. D.; Goepel, W. *Int. J. Quantum Chem.* **1997**, *62*, 427.
(8) McAdon, M. H.; Goddard, W. A., III. *Phys. Rev. Lett.* **1985**, *55*, 2563.
(9) Gupta, S. K.; Nappi, B. M.; Gingerich, K. A. *Inorg. Chem.* **1981**, *20*, 966.
(10) Lide, D. R. *Handbook of Cemistry and Physics*, 71st ed.; CRC Press: Boca Raton, 1990−1991.
(11) Dai, D.; Balasubramaniam, K. J. *J. Chem. Phys.* **1995**, *103*, 648.
(12) Yang, S. H.; Drabold, D. A.; Adams, J. B.; Ordejon, P.; Glassford, K. *J. Phys.: Condens. Matter* **1997**, *9*, L39.
(13) Ellis, D. E.; Guo, J.; Cheng, H. P.; Low, J. J. *Adv. Quantum Chem.* **1991**, *22*, 125.
(14) Bigot, B.; Minot, C. *J. Am. Chem. Soc.* **1984**, *106*, 6601.
(15) An equilvalent resonance structure would have doubly occupied IBO in the *other* half of the tetrahedra. Another picture of this could be to have singly occupied tetrahedral interstitial orbitals in all the tetrahedra. We have chosen to formulate the model in terms of one resonant structure, since the electron configuration remains unaffected.
(16) Leschik, G.; Courths, R.; Wern, H.; Hufner. S.; Eckardt, H.; Noffke, J. *Sol. State Commun.* **1984**, *52*, 221.
(17) Davenport, J. W.; Watson, R. E.; Weinert, M. *Phys. Rev. B* **1985**, *32*, 4883.
(18) Pandya, R. K.; Joshi, K. B.; Jain, R.; Ahuja, B. L.; Sharma, B. K. *Phys. Status Solidi B* **1997**, *200*, 137.
(19) Richter, L. J.; Ho, W. *Phys. Rev. B* **1987**, *36*, 9797.
(20) Pipek, J.; Mezey, P. G. *J. Chem. Phys.* **1989**, *90*, 4916.
(21) Slater, J. C. *Quantum Theory of Molecules and Solids: The Self-Consistent Field for Molecules and Solids*; McGraw-Hill: New York, 1974; Vol. 4.
(22) Perdew, J. P.; Chevary, J. A.; Vosko, S. H.; Jackson, K. A.; Pederson, M. R.; Singh, D. J.; Fiolhals, C. *Phys. Rev. B* **1992**, *46*, 6671.
(23) Moore, C. E. *Atomic Energy Levels*; National Bureau of Standards: Washington, DC, 1971; Vol. III.
(24) *Jaguar 3.0*; Schrödinger, Inc.: Portland, OR, 1997. *PS-GVB*, version 2.3; Schrödinger, Inc.: Portland, OR, 1996.
(25) Hay, P. J.; Wadt, W. R. *J. Phys. Chem.* **1985**, *82*, 299.
(26) Becke, A. D. *Phys. Rev. A* **1988**, *38*, 3098.
(27) Vosko, S. H.; Wilk, L.; Nusair, M. *Can. J. Phys.* **1980**, *58*, 1200.
(28) Lee, C.; Yang, W.; Parr, R. G. *Phys. Rev. B* **1988**, *37*, 785.